Available online at www.sciencedirect.com
SCIENCE DIRECT®
PERGAMON
International Journal of Heat and Mass Transfer 46 (2003) 2291–2303
International Journal of HEAT and MASS TRANSFER
www.elsevier.com/locate/ijhmt

Evaluation of the radiative properties of a dispersed particulate medium for construction material applications

Bonnie K. Wiseman, Jamil A. Khan *

Laboratory for Applied Heat Transfer, University of South Carolina, Columbia, SC 29208, USA

Received 29 January 2002; received in revised form 13 September 2002

Abstract

Recent studies have suggested that the heat buildup of construction materials may be significantly reduced, without affecting the material color, by the incorporation of scattering particles.

The scattering particles were found to alter the near infrared diffuse reflectance of the material, depending on their refractive index, volume percent, and particle size combination. In addition, a theoretical model was developed and correlated well with the experimentally measured values, accurately predicted increases in diffuse reflectance and drops in temperature. Thus, the model may be effectively used to design dark colored polymeric materials with reduced heat buildup properties.

Keywords: Radiative; Dispersed; Scattering; Particulate medium; Building material

1. Introduction

Recent research on construction materials has shown that, depending on the pigment system used to impart color, a significant temperature rise may occur due to absorption of infrared radiation [1]. Current trends in the building products industry suggest that consumers prefer to use darker colors for many applications. However, it is well known that darker colors tend to absorb more of the sun's energy. Excessive temperature rise above the polymer's glass transition temperature often results in failure of the parts while in service. ASTM D4803-93, standard test method for predicting heat buildup in PVC building products, was developed to try to prevent these service failures from happening in the field. Correlations between solar reflectance measurements and heat buildup may also be used to predict the maximum service temperature [1]. However, it would also be beneficial if there were a predictive model available for use in the formulation design process that would predict temperature rise based on formulation components alone.

Methods for improving the dimensional stability of dark colored polymeric materials have historically focused on increasing the material's modulus with reinforcing fillers or with heat distortion modifiers. However, these solutions negatively affect other elements of the system, such as, impact properties and cost. Other studies have suggested that the infrared reflectance of a pigment/polymer system may be enhanced by the incorporation of scattering particles that are transparent at certain infrared wavelengths, thus reducing the energy absorption of the material at those wavelengths, and thereby reducing the temperature rise [1,2]. It has been found that any material which is transparent to infrared radiation in the required spectral range, and which also has a refractive index substantially different from its binder's refractive index, may be used as an infrared reflecting particle [2]. However, these particles must not interfere with reflectance in the visible part of the spectrum so that the desired color is maintained.

The solution for light scattering by a homogeneous sphere was developed by Gustuv Mie in 1908 [3]. When using this theory it is assumed that only single, independent scattering exists. The theory involves the

* Corresponding author. Tel.: +1-803-777-1578; fax: +1-803-777-0106.
E-mail address: jamil.khan@sc.edu (J.A. Khan).

0017-9310/03/$ - see front matter
doi:10.1016/S0017-9310(02)00511-2

Nomenclature

β	extinction coefficient $= \kappa + \sigma_s$
Φ	scattering phase function—describes the probability that a ray from one direction *si*, will be scattered into a certain other direction *s*
φ	azimuthal angle
κ	the absorption coefficient
μ	cosine of the scattering angle
Θ	scattering angle
θ	polar angle
σ	scattering coefficient
τ	optical depth
$d\Omega$	solid angle $= \sin\theta_i\, d\theta_i\, d\varphi$
ω	the scattering albedo
I	local intensity at location **s**
s	general direction of propagation
z	perpendicular position of intensity with in a plane parallel medium
$I(si)$	in-coming scattering intensity
si	in-coming scattering directions
Ib	black body intensity

Subscript

i	in-coming radiation

solution of the scattering phase function, the degree of polarization, and the scattering efficiency for a homogeneous sphere. In general, Mie scattering applies for a size parameter (x) in the range $0.3 < (x = \pi D/\lambda_{vac}) < 5$, where D is the diameter of the sphere and λ_{vac} is the wavelength of light in a vacuum [4]. However, energy absorption by the medium, absorption by the particles, or both can be accounted for in this theory, and the results apply over the entire range of particle diameters. If the absorptive index, k, is small ($\ll 1$) and kx is $\ll 1$, then larger spheres can be treated with the Mie theory as well [5]. A Fortran subroutine for solving the Mie equations has been developed for a non-absorbing sphere in a medium with refractive index of unity [4]. For large spheres, where $x \gg 1$, the scattering is essentially a reflection process, which can be calculated from simple geometric reflection relations [5].

Many studies have utilized the Mie theory for determining the radiation transfer of thin films with very low concentrations of homogeneous spheres, where they have assumed only isotropic independent scattering and non-reflecting boundaries [6–11]. Single scattering applies if a single ray of light traversing through a volume of scatterers is scattered only once before leaving the medium [10]. However, in most practical applications, this is not the case. In the likely occurrence of multiple scattering, energy scattered from one particle can hit another and be scattered additional times before it exits the medium. One theoretical check for single scattering conditions that can be made is to calculate the optical path, which is the product of the scattering coefficient and the slab thickness. If the optical path is less than 0.1, single scattering can be assumed. The calculations for reflected energy are greatly simplified for single scattering systems, as the scattered intensity of the system is simply the sum of the scattered intensities from the individual particles [10]. However, it has been shown that an incoming scattering term may be added in the equation of radiative transfer to account for multiple scattering [6].

As was mentioned, in addition to single scattering, another key assumption used in the studies above is that of independent scattering. Independent scattering applies for conditions where the clearance between particles is large compared to the sphere diameter and wavelength of radiation. However, studies on paint layers have shown that the independent single scattering assumption may not be sufficient to obtain the correct solution of the radiative transfer equation [6,8,10,12–14]. These studies indicate that it is likely that dependent scattering will occur when the scattered electromagnetic fields of particles interfere with each other due to an increasing volume concentration of particles. As the volume concentration of pigment is increased, the spacing between particles is reduced. The interference that results from this close spacing causes scattering coefficients to decrease and absorption coefficients to slightly increase [12]. Kumar and Tien [14] developed a scattering regime map as a function of particle size parameter and volume fraction for various types of scattering. Their results show that pigment dispersions may potentially fall in either the independent or dependent scattering range depending on the particle size and volume fraction. Specifically, for volume fractions at less than 10% and for particle size parameters greater than 1, it is likely that independent scattering exists [6].

In their study, Hottel et al. [11] predicted the reflection properties for a non-absorbing medium containing non-absorbing spheres for single scattering, multiple scatter for open-spaced particles, and multiple scatter for close-packed systems. In comparing their experimental results, an empirical equation for predicting the interference for a multiple, dependent scattering system was developed. This equation enables the use of existing theory to calculate the bi-directional reflectance of close packed spheres with good correlation to measured val-

ues [8]. Essentially, the Mie equations are used to calculate the scattering efficiency for the single scatter case and an empirical relation is then used to determine an effective scattering efficiency.

Shafey and Kumitomo [7] conducted a similar study for an absorbing medium containing a high concentration of non-absorbing and scattering particles of pigment. The study results indicate that as the volume percent of particles increases, the difference in diffuse reflectivity between measured values and those calculated using the Mie coefficients (independent scattering) increases as well. They found that the empirical equation for the interference effect mentioned above, which was developed for pure scattering, was also in good agreement with their results for a multiple and dependent scattering–absorption system.

Varandan and coworkers [15] took the analysis further to assess a heterogeneous medium in which there is absorption by the matrix and the particles, where multiple and dependent scattering exists. Their research suggests that an effective propagation constant is needed to adequately describe the radiation as it propagates through such a heterogeneous medium. Thus, the effective scattering efficiencies for this case can be determined in terms of the effective propagation constant to account for the enhanced absorption associated with dependent scattering. In the solution, it is assumed that the wavelength in the matrix material is much larger than the size of the particles and results in a very small non-dimensional frequency, which happens to fall in the Raleigh region. However, the authors mention that with considerable computational effort, this analysis can be extended to Mie particles as well. The results of this study quantitatively illustrate that enhanced absorption, due to dependent scattering, may greatly affect the diffuse reflectance.

The isotropic scattering assumption used in the Mie scattering analysis is often an idealization. The more common problem of anisotropic scattering has generally been avoided due to the complexities associated with the analysis. Many researchers, such as Chandrasekhar [16], and Love and Grosh [17] have solved the integro–differential equations by Gaussian quadrature. Even with a simple one-dimensional model, such as an isothermal slab, the exact solutions to higher-order anisotropic scattering require the solution of a four-term phase function. Yet, Bergquam and Seban [18] reported using simplified methods, such as the two-flux method, to deal with realistic scattering phase functions. Domota and Wang [19] used a modified two-flux method. Several researchers have used a more realistic and less cumbersome analysis of linear-anisotropic scattering [20,21]. Buckius and King [22] used the exponential kernal method combined with linear-anisotropic scattering to predict diffuse solar radiation. Dayna and Tien [23] also applied this method to a gray slab at radiative equilibrium. Modest and Azad [20] demonstrated that the approximation of the phase function by linear anisotropic scattering yields results of excellent accuracy for isothermal slabs and slabs at radiative equilibrium.

2. Theoretical development

2.1. Physical model

In general, the physical model for this analysis may be considered an optically thick, one-dimensional plane-parallel medium consisting of a polymer matrix containing evenly distributed pigment particles. Scattering particles of different size and relative refractive index were added to the pigmented medium, and their influence on the infrared diffuse reflectance and temperature was assessed. The schematic shown in the Fig. 1 illustrates the physical model for the analysis.

2.2. Overall energy balance and equation of transfer

For the one-dimensional plane-parallel medium described above, the direction of the intensity, as it moves through the medium, is measured by the polar angle, θ, as measured from the perpendicular direction (z), and the azimuthal angle, φ, in the x–y plane. However, if it is assumed that the temperature field and radiative properties of the medium vary only in the perpendicular direction, the radiative intensity does not depend on azimuthal angle and the overall energy equation reduces to,

$$0 = \frac{\mathrm{d}q}{\mathrm{d}z} = \frac{\mathrm{d}}{\mathrm{d}z}\left[\frac{-k\,\mathrm{d}T}{\mathrm{d}z} + q_{\mathrm{r}}\right] \tag{1}$$

where q is the heat flux, k is the thermal conductivity of the material and T is the temperature. Therefore, if an expression for the radiative heat flux, q_{r}, is known, the temperature distribution across the z direction may be derived.

In general, the radiative heat flux, may be expressed in terms of local radiative intensity, $I(\tau,\theta)$, where τ is the optical depth and θ is the polar angle.

$$q_{\mathrm{r}}(\tau) = 2\pi\int_0^{\pi} I(\tau,\theta)\cos\theta\sin\theta\,\mathrm{d}\theta \tag{2}$$

Therefore, to develop a model to predict temperature, the equation of transfer must be solved. The equation below is the integrated form of the equation of transfer for a plane parallel medium [5]:

$$I(\tau,\theta) = I(0)\,\mathrm{e}^{-\tau} + \int_0^{\tau} S(\tau',\theta)\mathrm{e}^{-(\tau-\tau')}\,\mathrm{d}\tau' \tag{3}$$

Physically, this equation shows the contribution to the local intensity by the intensity entering the medium at

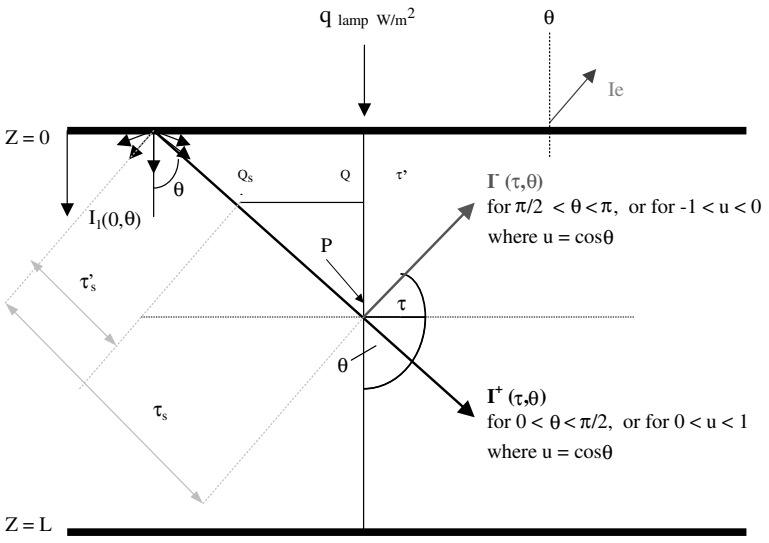

Fig. 1. Schematic of a one-dimensional plane parallel medium.

the surface ($z = 0$). As the intensity travels through the medium in some direction, θ, it decays exponentially due to extinction over the optical distance. The integrand in the second term, contains the source function, $S(\tau', \theta)$, which is the contribution from the local emission and in-scattering at τ'. This term is attenuated exponentially by self-extinction over the optical distance between the emission point and the point under consideration $(\tau - \tau')$. The integral sums the contributions over the entire emission path.

The source function may be expressed as [5]:

$$S(\tau', \theta) = (1 - \omega) I_b(\tau') + \frac{\omega}{2} \int_0^{\pi} I(\tau', \theta_i) \Phi(\theta, \theta_i) \times \sin\theta_i \, d\theta_i \quad (4)$$

In this equation, $I(\tau', \theta_i)$ is the in-scattering intensity at the point of origin of the source, τ', ω is the scattering albedo, I_b is the black body intensity, and $\Phi(\theta, \theta_i)$ is the scattering phase function.

2.3. Model equations

The general equation of transfer, Eq. (3), was modified for the polymeric medium described above. Assuming a cold medium, the first term on the right hand side of the source function term, Eq. (4), is neglected. Thus, the source function is due only to the in-scattering intensity. The only radiative source available to produce the in-scattering comes from the external source. Some of the lamp intensity is reflected at the surface and the rest is attenuated over the optical depth to the position where the in-coming scattering source originates, τ'. Therefore, the source function and local intensity reduce to the following equations, which are also a function of wavelength:

$$S(\tau')_\lambda = (1 - \rho) \frac{q_l}{\pi} \Phi_\lambda e^{-\tau'/u} \quad (5)$$

$$I+(\tau, u)_\lambda = I_l(0) e^{-\tau/u} + \int_0^{\tau} (1 - \rho) \frac{q_l}{\pi} \Phi_\lambda e^{-\tau/u} e^{-(\tau - \tau')/u} \frac{d\tau'}{u} \quad (6)$$

$$I-(\tau, -u)_\lambda = -\int_0^{\tau L} (1 - \rho) \frac{q_l}{\pi} \Phi_\lambda e^{-\tau/u} e^{-(\tau L - \tau)/u} \frac{d\tau'}{-u} \quad (7)$$

for $0 < (u = \cos\theta) < 1$.

In these equations, ρ is the reflectance at the surface of the slab, as determined from the Fresnel equation, q_l is the radiation source, and Φ_λ is the spectral scattering phase function. Eq. (6) shows the local intensity limited to directions emanating from the upper interface traveling in "positive" (downward) directions for $0 < \theta < \pi/2$, and $I_l(0, \theta)$ is the intensity at the top surface at $\tau = 0$. Eq. (7) shows the local intensity limited to "negative" (upward) directions for $\pi/2 < \theta < \pi$. In order to solve the equation of transfer and complete the temperature calculation, the optical depth and scattering phase function must be determined.

To determine the optical depth and scattering phase functions for small particles of size 1 to 20 μm, Bohren's Mie Fortran program was modified to include a distribution of particles sizes for wavelengths from 350 to 2600 nm [10]. The Mie scattering efficiencies, Q_{sca}, were used to determine the Mie scattering coefficients, σ_s, and therefore, the optical depth, τ. To account for the distribution of sphere particle sizes, the scattering coefficient was first integrated over the radius range to give

spectral scattering coefficient, $\sigma_s(\lambda)$. The total optical depth was then determined by integrating over the entire wavelength range.

$$\sigma_s(\lambda) = \pi \int_0^\infty Q_{sca}(a,\lambda) a^2 n(a)\,da \tag{8}$$

$$\tau = L \int_{350\,nm}^{2600\,nm} \sigma_s(\lambda)\,d(\lambda) \tag{9}$$

Similarly, the Mie Fortran program was used to determine the scattering phase functions, as a function of radius and wavelength. As described by the equation below, the scattering phase function is first calculated for each sphere radius and wavelength combination, for angles from 0° to 180°. By integrating over the particle size range, the dependence on radius maybe be accounted for, yielding a scattering phase function that is dependent on wavelength and scattering angle only,

$$\Phi(\Theta)_\lambda = \frac{\pi}{\sigma_\lambda} \int_0^\infty Q_{sca} a^2 \Phi(\Theta,a,\lambda) n(a)\,da \tag{10}$$

For large particles of sizes 88 to 106 μm, large sphere scattering theory was applied for both specular and diffuse sphere assumptions. The specular scattering phase function is determined from the following equation, where ρ^s is the hemispherical specular reflectivity for a large specular sphere and Θ is the scattering angle,

$$\Phi(\Theta) = \rho^s \frac{(\pi - \Theta)}{2} \tag{11}$$

Also, since ρ^s is equal to the scattering efficiency of the system, the scattering coefficient may be found from the following equation for a distribution of particles $n(a)$:

$$\sigma_s(\lambda) = \pi \rho^s \int_0^\infty a^2 n(a)\,da \tag{12}$$

For a large diffuse sphere, the scattering efficiency is equal to the hemispherical reflectivity of the sphere and is substituted into Eq. (12) to determine the diffuse scattering coefficient. The diffuse scattering phase function is shown below [24,25]:

$$\Phi(\Theta) = \frac{8}{3\pi}(\sin\theta + \theta\cos\theta) \tag{13}$$

It has been shown in the literature that linear approximations of exact scattering phase functions may be used with good results [5]. By choosing appropriate forward (or backward) scattering cut-off angles and taking a linear approximation of the resulting curve, the theoretical scattering phase function curves for Mie particles may be approximated. Modest and Azad suggest using the double Dirac function as follows [20]:

$$\Phi(\Theta) = 2f\delta(1-\mu) + 2b\delta(1+\mu) + (1-f-b)\Phi^*(\Theta) \tag{14}$$

$$\Phi^*(\Theta) = 1 + A_1^* P_1(\mu) \tag{15}$$

In the above equations, f is the forward-scattered fraction of energy. The expression, $(1-f)$, is equal to $\Phi^*(0°)$, the value of the linear scattering phase function with the scattering angle equal to zero ($\Theta = 0°$). The value of b is the fraction of energy scattered in the backwards direction ($\Theta = 180°$), usually zero except for large diffusely reflecting particles; A_1^* is the slope of the line, and $P_1(\mu)$ is the first order Legendre polynomial of μ, the cosine of the scattering angle.

To account for other than isotropic scattering, and if there is no appreciable backscattering ($b = 0$), the equation of transfer may be easily modified by replacing $\Phi(\Theta)$ in Eq. (1) with the linear-anisotropic scattering phase function (Φ^*). In this case, the fraction of forward scattered intensity is treated as transmitted and the scattering coefficient (σ_s) may be replaced with an effective scattering coefficient $\sigma_s^* = (1-f)\sigma_s$ [5]. The effective scattering coefficient is also used in the determination of the optical depth (τ).

Once the radiative transfer equation is solved, the temperature of the polymeric sheet may be determined by deriving the temperature profile from the solution of Eqs. (1) and (2). The resulting temperature profile was found to be:

$$T = \left(2\alpha q_{lamp}\frac{\Phi_t}{k\sigma_s}\right)\left[-e^{-\sigma_s z} - \sigma_s z e^{-\sigma_s z} - e^{-\sigma_s z} - e^{-2\sigma_s L + \sigma_s z} + e^{-\sigma_s L + \sigma_s z}\right] + \frac{C_1 z}{k} + C_2 \tag{16}$$

where, α is the absorptivity, Φ is the value of the scattering phase function in the forward direction ($u = 1$), σ_s is the total scattering coefficient, and C_1 and C_2 are constants.

To complete the temperature calculation, the boundary conditions must be considered as follows:

$$\text{At } z = L, \quad \frac{dT}{dz} = 0 \tag{17}$$

$$\text{At } z = 0, \quad T(0) = T_e = \left[\frac{\alpha q_l}{\varepsilon\sigma}\right]^{1/4} \tag{18}$$

where T_e is the equilibrium upper surface temperature determined from the surface energy balance. In Eq. (15), q_l is the radiation source, ε is the known emissivity of the material, α is the absorptivity of the material and σ is the Stefan–Boltzman constant.

Therefore, for the upper surface, as the negative traveling intensity propagates through the medium, it will encounter the upper interface where part of the intensity will be reflected back into the medium as the specular reflectivity, R_s, as described by Snell's law and the Fresnel equation. The intensity that is refracted at the interface is the emergent intensity, I_e, which may be defined in terms of the negative traveling intensity at the surface ($\tau = 0$):

$$I_e = \frac{[1 - R_s(S')]}{n_2^2} I - (0) \tag{19}$$

where n is the refractive index of the polymeric medium. The bi-directional diffuse reflectivity was determined by the following equation:

$$r_d = \frac{\pi I_e}{I_0} \tag{20}$$

The hemispherical diffuse reflectance, R_d, was determined by integrating bi-directional diffuse reflectivity (r_d) over the hemisphere. Thus the value of the spectral absorptivity (α_λ) may be determined from the following equation:

$$\alpha_\lambda = 1 - (\rho_\lambda + R_{s\lambda} + VR_{d\lambda}) \tag{21}$$

In this equation, ρ_λ is the known diffuse reflectance value of the pigmented matrix material, $R_{s\lambda}$ is the calculated spectral specular reflectance at the upper interface, and $\Delta R_{d\lambda}$ is the spectral diffuse reflectance difference which was calculated as outlined above. This value represents the change in diffuse reflectance of the pigmented matrix material due to the addition of the scattering spheres.

Using the equations above, the diffuse reflectance difference and temperature profile across the slab were determined and compared to the actual experimental values.

3. Experimental design

3.1. Materials

Two compositions of scattering particles, with differing refractive index, and various particle size ranges were selected for this study. The materials are listed below:

Georgia Gulf substrate compound—1% TiO_2 blue pigment
microsphere composition:
GL-0191 (refractive index = 1.51)
GL-0176 (refractive index = 2.1)

The control formulation, consisting of the polymer compound and 1% blue pigment, was used as the medium for the various microsphere formulations. The refractive index (n) of this material was found to be 1.59 through Ellipsometry testing. All formulations were prepared in duplicate and were processed on a two-roll mill at 360 °F and were pressed into a plaque 70 mils (0.1778 cm) in thickness. The microsphere formulations are listed in Table 1.

Table 1
Microsphere formulations

Microspheres	Refractive index	Particle size range (μm)	Volume percent
GL-0176-Mie	2.1	1–20	10
GL-0176-Large	2.1	88–106	10
GL-0191-Mie	1.51	1–15	10
GL-0191-Large	1.51	88–106	10

3.2. Experimental testing and results

The samples were evaluated for diffuse reflectance as a function of wavelength, up to 2600 nm, using an integrating sphere spectrophotometer. The statistical significance of the data was also assessed. Fig. 2 shows the percent reflectance curves for the two Mie particle formulations versus the control formula. The figure shows that the addition of the GL-0176-Mie spheres to the control medium provided an increase in infrared reflectance.

Fig. 3 shows the percent reflectance curves for the two large sphere formulations. The curves show that for both large sphere formulations, there is a decrease in the percent reflectance over wavelength ranges from 700 to

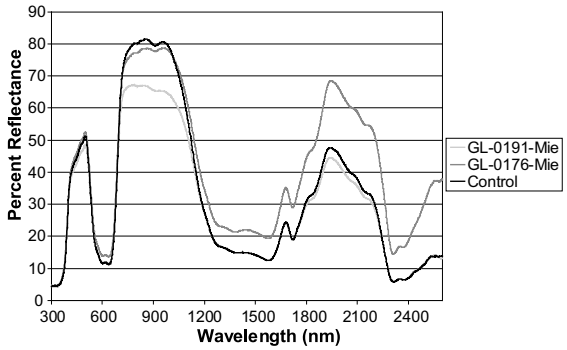

Fig. 2. Percent reflectance for Mie particle formulations of GL-0191-Mie.

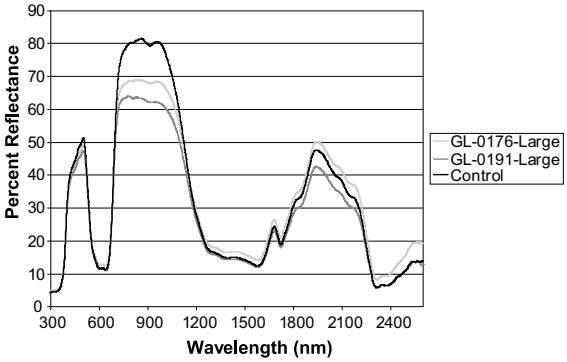

Fig. 3. Percent reflectance for large sphere formulations of GL-0191-Large and GL-0176-Large spheres.

Table 2
Summary of results for reflectance test

Formula	Sphere refractive index	Particle size (μm)	NIR reflectance (%)	Standard deviation
GL-0176-Mie	2.1	1–20	35.3	0.1
GL-0176-Large	2.1	88–106	24.3	0.1
GL-0191-Mie	1.51	1–15	24.8	0.4
GL-0191-Large	1.51	88–106	23.7	0.6
Blue control			27.4	0.2

1200 nm. The data presented in both figures was integrated over the wavelength range of 700–2600 nm to obtain the total reflectance for the NIR region.

From the statistical analysis of the data, it was found that the GL-0176 formulation was statistically different, to a 95% confidence level, from the control due to increased infrared reflectivity. These results are summarized in Table 2 and show that the sample preparation and test method were reproducible.

Temperature rise testing was conducted on the four formulations versus the control using ASTM D4803-93: standard method for predicting heat buildup in PVC building products. In the test, a 250 w infrared lamp is used to simulate energy from the sun. Previous work has shown that the temperature rise test has an inverse correlation of 95% with reflectance data—the higher the reflectance values, the lower the temperature rise. In previous studies, this test was also found to be reproducible and to correlate with actual sun exposure [1,26].

The bottom surface temperature of each sample was recorded as a function of time versus a black body. The surface temperatures were normalized using the black body temperatures measured during each test so that the individual test data may be directly compared. The data is also summarized in Table 3.

4. Comparison of theory and experiment

4.1. GL-0176-Mie spheres (1–20 μm)

The results from the Mie program indicate that both the scattering coefficient and the forward scattering phase function vary with wavelength and particle size. On a spectral basis, the scattering was most efficient when the particle and wavelength were of similar size.

Table 3
Temperature rise test results

Formulation	Measured equilibrium temperature (°C)
Blue control	122.4 (395.5 K)
GL-0176-Mie	114.5 (387.6 K)
GL-0176-Large	124.8 (398 K)
GL-0191-Mie	123.5 (396.7 K)
GL-0191-Large	125.5 (398.6 K)

Similarly, for the entire distribution of particles, the highest wavelength was found to provide the largest forward scattering value. In fact, the highest diffuse reflectance difference and the highest forward scattering phase function was found to occur at 2600 nm. This would suggest that reflectance would increase if smaller particles of this composition were used in the formulation.

The phase function plots also revealed that as the wavelength increases, the level of transmitted intensity, as indicated by the value of $(1 - f)$, decreases. Thus, the intensity goes from being 100% transmitted, i.e., scattered in the direct forward direction, to having a larger fraction if intensity scattered in a linear-anisotropic fashion. The analysis of the total scattering phase function plot reveals that for the refractive index, particle distribution and particle density in question, linear-anisotropically scattered fraction is 0.2%. This result is illustrated in Fig. 4.

Fig. 5 illustrates a comparison of the theoretical and experimental diffuse reflectance difference for the GL-0176-Mie sample versus the control formulation. The figure shows that the increase in reflectance due to the addition of the GL-0176-Mie microspheres was predicted using the model and correlates with the increased reflectance values as measured by the Shimadzu spectrophotometer. These spectral values were then integrated over the entire wavelength range to obtain the total diffuse reflectance difference. The percent error between the calculated and experimental diffuse

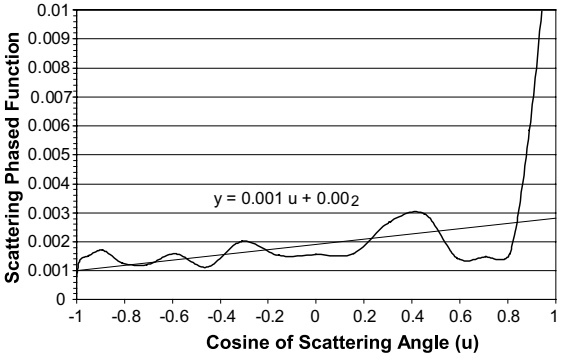

Fig. 4. Wavelength integrated Mie scattering phase function for GL-0176-Mie spheres of 1–20 μm.

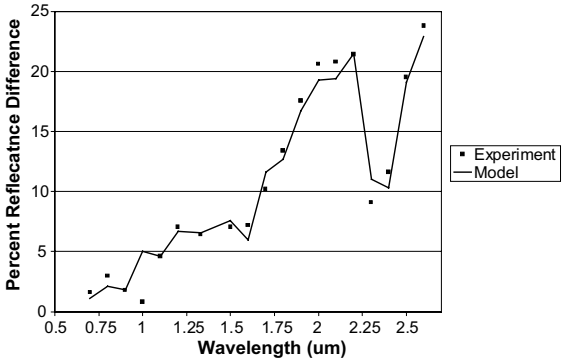

Fig. 5. Diffuse reflectance difference comparison GL-0176-Mie spheres of size 1–20 μm minus control material.

reflectance difference was only 0.3%. These results suggest that 0.2% linear-anisotropic scattering was enough to provide this 10.6% increase in diffuse reflectance.

4.2. GL-0191-Mie spheres (1–15 μm)

The sample containing the GL-0191-Mie particles was found to have less scattering efficiency than the GL-0176 sample, as shown by comparing the forward scattering peaks and the forward scattering fractions in Figs. 6 and 4, respectively. The results indicate that almost all of the intensity is transmitted directly in the forward direction for the GL-0191-Mie spheres. This result directly impacts the bi-directional reflectivity. The only source of radiation for the negative traveling intensity comes from the intensity that penetrates into the medium from the external source at the top surface. This intensity is scattered at the particle–medium interface and is subsequently redirected in a fashion illustrated by the scattering phase function. If this scattering is negligible, then the negative traveling intensity is negligible. This result may be due to the fact that the refractive index of these spheres are very close to that of the wavelength averaged refractive index of the medium.

Therefore, as was expected, the addition of the GL-1091 spheres resulted in a negligible emergent intensity and therefore a negligible diffuse reflectance difference. The experimental reflectance results for this sample were found to be statistically the same as that of the control formulation. However, as illustrated by Fig. 7, this application of the Mie theory will only predict an increase in reflectance. As shown by the curve representing the measured values of reflectance, the addition of the GL-0191-Mie spheres caused a decrease in reflectance at several wavelengths. Where the control sample had higher reflectivity, the calculated reflectance difference was found to be negligible. However, at wavelengths of 2.4 and 2.5 μm, where the addition of the GL-0191-Mie spheres did increase the reflectivity, the calculated values predicted this slight increase. Thus, this method of prediction of diffuse reflectance will not provide an indication of a reflectivity reduction, only an increase.

For both samples, the total diffuse reflectance difference values and the total effective scattering coefficient were used in the temperature calculation. Table 4 summarizes the theoretical model and experimental results for both the GL-0176-Mie and GL-0191-Mie samples.

4.3. Large spheres (88–106 μm)

To check the large sphere assumption for the remaining formulations, the diffuse and specular cases for large spheres were assessed. The formulations containing spheres of size 88–106 μm have very large size parameters—on the order of 100. For these spheres, the laws of geometric optics may be used to determine the scattering coefficients and phase function. Depending on the type of reflection at the sphere–medium interface, the reflection may either be diffuse or specular in behavior.

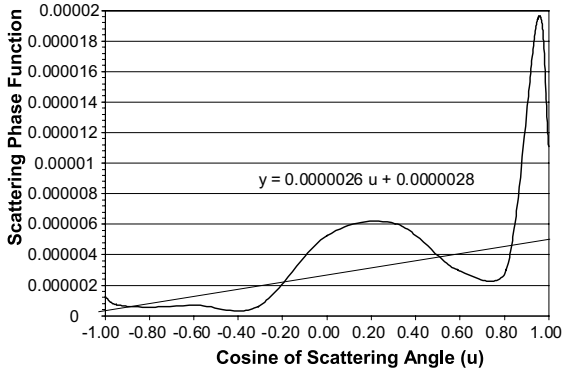

Fig. 6. Wavelength integrated Mie scattering phase function for GL-0191-Mie spheres of 1–15 μm.

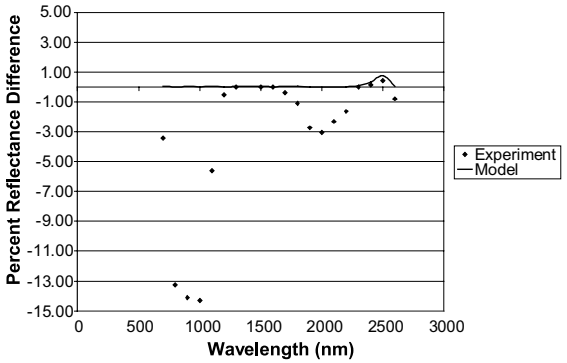

Fig. 7. Diffuse reflectance difference comparison GL-0191-Mie spheres of size 1–15 μm minus control material.

Table 4
Summary of Mie scattering analysis results

Property	GL-0176	GL-0191
Forward scattering fraction f (%)	99.8	~100
ΔR_d calculated (%)	10.64	0.084
ΔR_d measured (%)	10.61	−3.27
Calculated temperature (K)	387.5	404.4
ΔT (K) (calculated − measured)	0	7.8

For a diffusely reflecting sphere, there is a large back scattering component to the scattering phase function, and very little forward scattering. It is possible to imagine that as the radiation interacts with a diffuse sphere, a large portion of that scattered intensity is redirected at 180°, which would be the negative traveling direction. However, when the negative traveling intensity interacts again with another sphere, it would then be redirected back again, thus resonating between spheres until the intensity is attenuated. This ultimately would lead to a limited source for the emergent intensity, and therefore a lower diffuse reflectance. The diffuse reflectance analysis used does not enable the calculation of a "negative" change in reflectance. However, for the GL-0176-Large sample, the calculated value of diffuse reflectance difference was negligible (0.004%) and the temperature was calculated to be essentially identical to the experimental value, with only 0.5% error. However, for the GL-0191-Large sample, the diffuse reflectance difference was found to be 1.6% and the temperature was predicted to be 3.5 °K higher than the experimental value. The fact that spectral data for the spheres was unavailable, forcing the use of total properties only, may be a source of error for this analysis.

Based on these results for the large two sphere formulations discussed above, it is likely to assume that the spheres under consideration may be diffusely reflecting. Fig. 8 shows the scattering phase function for a diffuse particle as determined via Eq. (13). Since the scattering behavior of a diffuse sphere is independent of the refractive index, this phase function may be applied to both GL-0176-Large and GL-0191-Large spheres. The diffuse reflectance difference, ΔR_d, and temperature were calculated via Eqs. (16)–(21).

Specular reflection occurs when the radiation is reflected back at the same angle of incidence for each location of the sphere surface. The spheres are assumed to be dielectric with the absorptive index essentially zero as compared to the refractive index n. However, k is assumed to be large enough to ensure that the spheres are opaque [5]. Specifically, for the specular case, spheres of refractive index $m = 1.51$ and 2.1 were compared.

For a specular reflecting sphere, there is a large forward scattering peak, which as determined in the Mie analysis, results in a high emergent intensity and a high diffuse reflectance. The two specular cases evaluated in the study, for a refractive index of 1.51 and 2.1, reveal that as the relative refractive index between the particles and the matrix increases, the greater the specular reflectivity is at the sphere–medium interface. Since this specular reflectivity is equal to the scattering efficiency of the system, the diffuse reflectance and therefore the temperature drop is directly affected by refractive index.

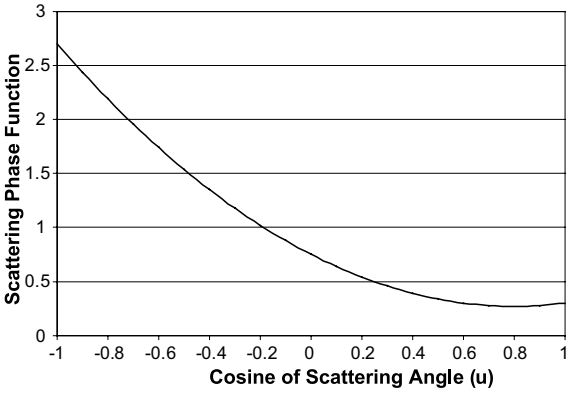

Fig. 8. Scattering phase function for a large diffusely scattering sphere.

For the GL-0191-Large spheres of refractive index 1.51, the specular reflectivity was very low, 1.5%. This result is due to the fact that the relative refractive index for the spheres and medium is very close to unity. Thus, there is very little redirection of intensity due to interaction at the interface of the medium and sphere. As a result, the forward fraction, f, of scattered radiation is 98%, and therefore, may be considered to be transmitted through the medium. Therefore the reflectivity and temperature results are not surprising that they appear to be similar to that found for the GL-0191 Mie case, which had the same refractive index and large forward scattered fraction as well.

In assessing the behavior of specularly reflecting spheres of greater refractive index, 2.1, Fig. 9 shows the greater scattering phase function. For the sample evaluated, even though the specular reflectivity was found to be only 6.4%, the value of $(1 - f)$ is 40%, thus leading to higher values of diffuse reflectance and a large temperature drop. Clearly in comparing these calculated results to the experimental analysis, the GL-0176-Large spheres selected do not show this type of scattering behavior. The calculated temperature drop was found to be 22.8 °K for specularly reflecting spheres of given particle density and refractive index 2.1, whereas the experimental data showed no appreciable difference from the control sample. Since spectral optical properties were not available for these spheres, only total properties were assumed and utilized in the analysis. Fig. 9 shows the scattering phase function and a linear approximation for specular spheres of refractive index 1.51 and 2.1.

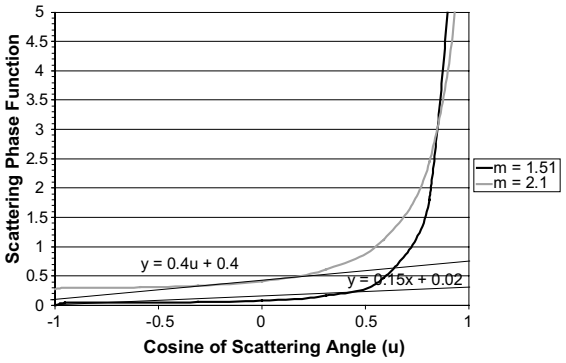

Fig. 9. Large sphere specular scattering phase function plots for GL-0176-Large and GL-0191-Large spheres of size 88–106 μm.

The linear-anisotropic approximations were used in the diffuse reflectance and temperature calculations. Table 5 below summarizes the results for the diffuse and specular large sphere analysis.

5. Case study

To further understand how refractive index and particle size may affect the scattering phase function, the Mie scattering efficiency (Q_{sca}) and scattering phase function data for the GL-0191-Mie and GL-0176-Mie spheres at a wavelength of 2.6 μm (and for a particle density of $N_t = 10^{-4}$ μm^{-3}) were compared to a theoretically designed particle of refractive index of 3.45 for two different particle size ranges. The results of this analysis are summarized in Table 6 and the phase function plot comparisons are shown in Figs. 10 and 11.

As shown in the Table 6, for the sample considered with an average particle size of 3.5 μm, the refractive index has very little effect on the scattering behavior of the spheres. Even though the GL-0176-Mie spheres show the greatest scattering efficiency, the forward scattering fractions are equivalent for all three materials, at 99.98%, indicating that most of the intensity would be transmitted for spheres of this size, refractive index, wavelength and particle density. Fig. 10 illustrates the similar scattering behavior for each refractive index case.

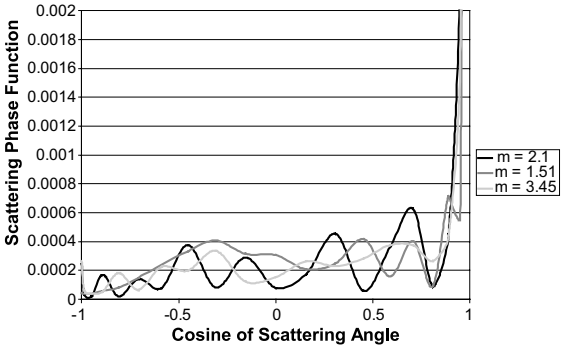

Fig. 10. Mie scattering phase function comparison for average particle radius = 3.5 μm and wavelength = 2.6 μm.

Table 5
Diffuse and specular scattering summary of results

Property	GL-0176 (88–106 μm)		GL-0191 (88–106 μm)	
	Specular	Diffuse	Specular	Diffuse
Forward scattering f (%)	60	~100	98	~100
ΔR_d calculated (%)	14.8	0.004	1.8	1.6
ΔR_d measured (%)	−2.03	−2.03	−3.71	−3.71
Calculated temperature (K)	374.4	396	401.8	402.1
ΔT (K) (calculated − measured)	−22.8	0.7	3.2	3.5
ΔT percent error (measured versus calculated)	5.9	0.5	0.8	0.9

Table 6
Mie theory comparison—effect of refractive index and particle size

	GL-0191 ($m = 1.51$)	GL-0176 ($m = 2.1$)	$m = 3.45$
For an average radius of 3.5 μm			
Scattering efficiency (Q_{sca})	1.34	3.29	2.85
Forward scattered fraction (%)	99.98	99.98	99.98
For an average radius of 0.5 μm			
Scattering efficiency (Q_{sca})	0.48	3.14	5.67
Forward scattered fraction (%)	88.44	40.66%	8.31%

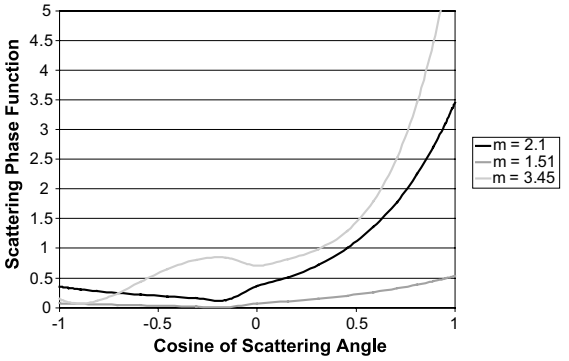

Fig. 11. Mie scattering phase function comparison for average particle radius = 0.5 μm and wavelength = 2.6 μm.

It should be noted that with a particle radius of 3.5 μm, the size parameter, even at a wavelength of 2.6 μm, falls outside of the typical Mie scattering range. However, for dielectric particles, this range may be extended by an order of magnitude in some cases [5]. Greater differences are seen between the different refractive index cases when the average particle size is assumed to be small. In this example, the theoretical (hypothetical) spheres showed a much higher efficiency and scattered fraction as compared to the other spheres.

In Fig. 11, the phase function for the $m = 1.51$ case shows very little scattering behavior versus the other refractive indices. The forward scattering fraction is 88.44%, indicating a large portion of the intensity is transmitted in the forward direction. The results from the reflectivity analysis above would suggest that this behavior would lead to low negative traveling intensity values and therefore low levels of diffuse reflectance. However, it is evident that the $m = 2.1$ case for this small particle size would be more effective at increasing the diffuse reflectivity than the actual sample evaluated which has a larger-size particle distribution. By reducing the particle size range from 3.5 to 0.5 μm, the forward scattering fraction would be reduced from 99.8% to 40.66%.

Thus, from this analysis, the theoretical sample with a refractive index of 3.45 and particle radius of 0.5 μm provides the greatest scattering efficiency, forward scattering peak and the lowest forward scattered fraction of only 8.31%. This indicates that most of the intensity would be scattered in a linear-anisotropic fashion, which would then provide the source of greater intensity in the negative traveling direction, thus leading to greater values of diffuse reflectance.

Since the reduction in temperature due to the GL-0176-Mie (1–20 μm) spheres was only 10.6 °K, the case for the theoretically designed spheres of refractive index 3.45 was evaluated further over the entire wavelength range. The calculated diffuse reflectance difference versus the control and the theoretical temperature drop was determined for this parametric design case. Fig. 12 shows the diffuse reflectance difference plot for these particles. The figure shows spectral diffuse reflectance differences approaching 50% versus the control material, with very little effect on reflectivity in the visible range of the spectrum (0.4–0.7 μm).

The Mie scattering phase function plot and its linear approximation are shown in Fig. 13. Table 7 summarized the wavelength integrated diffuse reflectance difference and scattering coefficient, the forward scattering phase function and the calculated temperature for this design case. As shown by Fig. 12 and the temperature drop shown in the table above, the higher refractive index and the smaller particle size of the theoretically designed particle offers improved performance versus the actual cases evaluated. The difficulty is in obtaining spheres of this limited particle size.

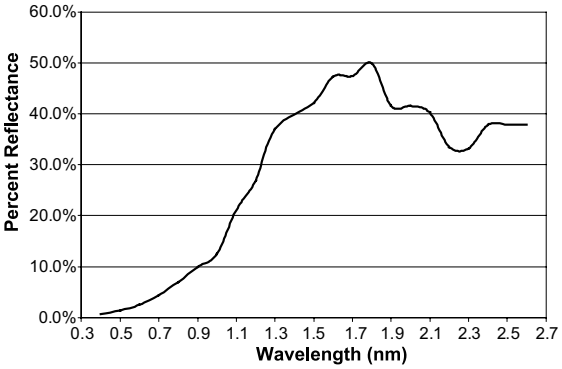

Fig. 12. Diffuse reflectance difference comparison for hypothetical particles $m = 3.45$ and particle radius = 0.5 μm.

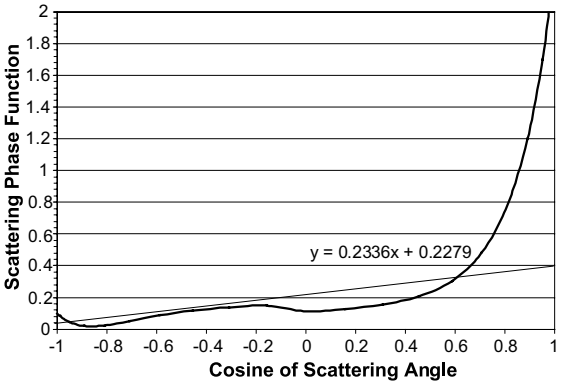

Fig. 13. Wavelength integrated scattering phase function for hypothetical particles of $m = 3.45$ and particle radius = 0.5 μm.

Table 7
Mie scattering results for designed scattering particles of $m = 3.45$

Forward scattered fraction (%)	77.21
Calculated total diffuse reflectance difference (%)	$\Delta R_d = 28.9\%$
Calculated temperature (K)	351.5
Temperature drop versus control (K)	44

6. Conclusions

In summary, to provide a dark colored polymeric material with minimal heat buildup, a Mie scattering particle approaching 0.5 μm in radius with a large relative refractive index is needed to optimize scattering in the near infrared part of the electromagnetic spectrum.

Similarly, for specular scattering, the higher the refractive index mismatch between the medium and spheres, the greater the scattering efficiency will be for the system. Specularly reflecting spheres have preferential scattering in the forward direction but as long as the majority of the radiation is not transmitted directly forward, the greater are the emergent intensity and diffuse reflectance. As with Mie scattering, specularly scattering particles may offer large temperature drops. However, the spectral optical properties are needed for the sphere to determine if it will affect the reflectance properties in the visible range of the electromagnetic spectrum.

Because diffusely reflecting particles have a large backscattering preference, they reduce the source of intensity for the negative traveling intensity. Thus, these systems offer reduced reflectivity and therefore higher temperatures.

The diffuse radiation at the upper surface of the slab is dependent upon how well the negative traveling intensity propagates through the medium. This intensity is highly dependent upon two key factors: (1) the available source for negative traveling intensity and (2) the scattering efficiency of the system. The source of intensity traveling within the medium originates from the external source at the top surface. However, to become a significant source for the negative traveling intensity, efficient scattering is required at the sphere–medium interface, and there must be a large fraction that is scattered other than in the direct-forward direction. In addition, there must be negligible back scattering. These factors directly affect the diffuse reflectance and the temperature of the material.

It has been found for this experimental and theoretical comparison that the combination of the modified Mie Fortran program and the linear-anisotropic scattering assumption enable an accurate prediction of values of increased diffuse reflectance and temperature drop. Therefore, this model may then be used to formulate dark colored polymeric materials with reduced temperature rise properties for building products applications.

Acknowledgements

The above research was funded by Americhem Inc., and SC EPSCoR funds.

References

[1] B. Wiseman, Absorption properties of building materials, Master's Thesis, University of South Carolina, 1998.
[2] P. Berdahl, Pigments to reflect the infrared radiation from fire, Energy & Environment Division, Lawrence Berkeley Laboratory, 1994.
[3] H.C. Van De Hulst, Light Scattering By Small Particles, John Wiley & Sons, 1957.
[4] C.F. Bohren, D.R. Huffman, Absorption and Scattering of Light By Small Particles, John Wiley & Sons, 1983 (Chapter 4).
[5] M.F. Modest, Radiative Heat Transfer, McGraw-Hill, 1993 (Chapter 8–12).
[6] R. Siegel, J.R. Howell, Thermal Radiation Heat Transfer, third ed., Hemisphere Publishing Corporation, 1992.
[7] H.M. Shafey, T. Kunitomo, Theoretical study on radiative properties of an optically thick painter layer containing spherical pigment (case of normal incidence), Bull. JSME 23 (182) (1980) 1366–1373.
[8] H.C. Hottel, A.F. Sarofim, W.H. Dalzell, I.A. Vasalos, Multiple scatter: comparison of theory with experiment, J. Transfer, Trans. ASME (May) (1970) 285–291.
[9] B.R. Palmer, P. Stamatakis, C.F. Bohren, G.C. Salzman, A multiple-scattering model for opacifying particles in polymer films, J. Coat. Technol. 61 (779) (1989) 41–47.
[10] C.F. Bohren, Multiple scattering of light and some of its observable consequences, Am. J. Phys. 55 (6) (1987) 524–532.
[11] H.C. Hottel, A.F. Sarofim, W.H. Dalzell, I.A. Vasalos, Optical properties of coating. Effect of pigment concentration, AIAA J. 9 (10) (1971) 1895–1898.
[12] C.L Tien, B.L. Drolen, Thermal radiation in particulate media with dependent and independent scattering, in: Annual Review of Numerical Fluid Mechanics and Heat Transfer, Vol. 1, Hemisphere, NY, 1987, pp. 1–32 (Chapter 1).
[13] T. Kumitomo, Y. Tsuboi, H.M. Shafey, Dependent scattering and dependent absorption of light in a fine-particle dispersed medium, Bull. JSME 28 (239) (1985) 854–860.
[14] S. Kumar, C.L. Tien, Dependent absorption and extinction of radiation by small particles, J. Heat Transfer, Trans. ASME 112 (February) (1990) 178–185.
[15] Y. Ma, V.K. Varandan, V.V. Varandan, Enhanced absorption due to dependent scattering, J. Transfer, Trans. ASME 112 (May) (1990) 402–407.
[16] S. Chandrasekhar, Radiative Transfer, Dover Publications, 1960 (Chapter II).

[17] T.J. Love, R.J. Grosh, Radiative heat transfer in absorbing, emitting, and scattering media, J. Heat Transfer, Trans. ASME (May) (1965) 161–166.
[18] J.P. Bergquam, R.A. Seban, Heat transfer by conduction and radiation in absorbing and scattering materials, ASME J. Heat Transfer 93 (1971) 236–239.
[19] G.A. Domota, W.C. Wnag, Radiative transfer in homogeneous nongray gases with nonisotropic particle scattering, ASME J. Heat Transfer C-96 (1974) 385–390.
[20] M.F. Modest, F.H. Azad, The influence and treatment of Mie-anisotropic scattering in radiative heat transfer, Trans. ASME 192 (February) (1980) 90–98.
[21] H.C. Hottel, A.F. Sarofim, L.B. Evans, I.A. Vasalos, Radiative transfer in anisotropically scattering media: allowance for Fresnel reflection at the boundaries, J. Heat Transfer, Trans. ASME (February) (1968) 56–62.
[22] R.O. Buckius, R. King, Diffuse solar radiation on a horizontal surface for a clear sky, Solar Energy 21 (1978) 503–509.
[23] A. Dayan, C.L. Tien, Radiative Transfer with anisotropicscattering in an isothermal slab, J. Quant. Spectrosc. Radiat. Transfer 16 (1976) 113–125.
[24] C. Chu, S. Churchill, Representation of the angular distribution of radiation scattered by a spherical particle, J. Opt. Soc. Am. 45 (11) (1955) 958–962.
[25] G.C. Clark, C. Chu, S. Churchill, Angular distribution coefficients for radiation scattered by a spherical particle, J. Opt. Soc. Am. 47 (1) (1957) 81–84.
[26] B. Wiseman, J.A. Khan, C.A. Rhodes, Experimental determination of absorption properties of building materials, in: Proceedings of the Third International Symposium On Radiative Transfer, Antalya, Turkey, 17–22 June 2001, pp. 641–651.